Materials Advances

ROYAL SOCIETY OF CHEMISTRY

PAPER

View Article Online
View Journal | View Issue

Cite this: *Mater. Adv.*, 2025, **6**, 1075

Poly(ethyleneimine)-exfoliated g-C_3N_4 nanosheets implanted in alginate beads and their application towards adsorptive desulfurization†

M. Christina Nilavu,[a] A. Santhana Krishna Kumar, *[b] Himanshu Aggarwal *[a] and N. Rajesh *[a]

Received 10th October 2024,
Accepted 10th December 2024

DOI: 10.1039/d4ma01020e

rsc.li/materials-advances

Advances in material science dictate the search for sustainable options that target diverse applications that impact climate change. In this context, we report the exfoliation and expansion of g-C_3N_4 using PEI polymer, followed by gelation as beads using calcium alginate for adsorptive desulfurization of thiophene compounds. Adsorbent characteristics were exemplified through FT-IR, FE-SEM-EDX, TGA, XRD, BET-N_2 isotherm, contact angle meter, XPS, HR-TEM, ZPC, and UTM. The PEI–g-C_3N_4 NSs@Ca-Alg bead composite with a mesoporous structure gave a specific surface area of 142.062 m^2 g^{-1} yielding a high adsorption capacity of 183.03 mg S g^{-1}. The material exhibited an ultimate tensile strength of 3500 kPa and a compressive stress of 527 kPa, accompanied by a compressive strain of 79%. The isotherm, kinetics, and thermodynamic investigations confirmed that the system exhibits pseudo-first-order kinetics and exothermic characteristics with spontaneity. The composite material had good potential for re-use for up to 5 adsorptive–desorption cycles with the potential to decrease the sulfur content to 58% in commercial diesel fuel.

1. Introduction

Combustion of automobile fuel causes sulfur pollution, a major environmental hazard. Therefore U.S. and European countries have been encouraging ultra low sulfur diesel (ULSD) parameters for diesel recently. However, permissible limits of sulfur in India according to BS(VI) have been reduced to below 10 mg L^{-1} for diesel fuel. In order to achieve the desirable limits, fuels that are separated from the crude oil are desulfurized before they are rendered commercially viable.[1,2] Sulfur is present as inorganic and organic forms in diesel oil. The major concern in the desulfurization process is the removal of organic sulfur compounds like thiophene (Tph), benzo-thiophenes (BT), dibenzothiophenes (DBT), and their derivatives as these molecules are highly non-polar with an electronegative sulfur atom.[3] In the conventional hydro-desulfurization process, a catalyst is used to break down aromatic carbon chains and remove sulphur as hydrogen sulphide (H_2S). This process has constraints in terms of high temperature and pressure, making it uneconomical for industrial use.[4] In addition the removal efficiency also decreases with an increase in the aryl ring on the thiophenic compounds. Alternative sulfur removal methods include extractive desulfurization, bio-desulfurization, and oxidative desulfurization. In extractive desulfurization, ionic liquids, amine-based solvents, DMSO, pyrrolidones, and polyethylene glycol (PEG) are used depending on their polarity and solubility to extract and remove aromatic sulphur compounds. However, this process is inefficient for large-scale applications due to more usage of organic solvents, which in turn makes the process less eco-friendly. Bio-desulfurization is yet another approach where biologically grown microorganisms are specifically cultured and used as a source for the removal of sulfur through different bio-enzymatic mechanisms. Although this method is a seemingly eco-friendly and cost-effective approach, selecting a suitable organism and their resistance to high temperatures makes it less effective for large scale application.[5] Adsorptive desulfurization could be explored as a comparatively better alternative for conventional hydrodesulfurization. In adsorptive desulfurization, the adsorbent could be tailored in terms of functionality, surface area, selectivity and reactivity according to the nature of the adsorbate. Regeneration capacity and reusability of the adsorbents make this process economically cost-efficient. Adsorbents synthesized from functionalized biopolymer and

[a] *Department of Chemistry, Birla Institute of Technology and Science-Pilani, Hyderabad Campus, Jawahar Nagar, Hyderabad 500078, India. E-mail: himanshu.aggarwal@hyderabad.bits-pilani.ac.in, nrajesh@hyderabad.bits-pilani.ac.in*

[b] *Department of Chemistry, National Sun Yat-sen University, No. 70, Lien-hai Road, Gushan District, Kaohsiung 80424, Taiwan. E-mail: krishnakumar@mail.nsysu.edu.tw*

† Electronic supplementary information (ESI) available. See DOI: https://doi.org/10.1039/d4ma01020e

natural sources are applicable in scale-up operations.[6] Biopolymer-based adsorbents as such are less appropriate for desulfurization owing to their low specific surface area and degradation temperature.[7] Previously, adsorbents including carbon materials,[8–10] zeolites,[11] cobalt-based metal–organic frameworks,[12] graphene, and graphene-based materials have been reported for desulfurization to overcome the above mentioned limitations.[13] Graphitic carbon nitride is a thermally stable, less-toxic and 2D layered material with high crystallinity and is not explored to its full potential for adsorptive desulfurization. In catalytic oxidative desulfurization, graphitic carbon nitride (g-C_3N_4) has been widely used.[14] The stable conjugated sp^2 configuration of carbon and nitrogen atoms in g-C_3N_4 forms a unique 2D layer structure of tri-*s*-triazine units.[15] These compounds can be effortlessly synthesized from precursors including thiourea, urea, melamine, and cyanamide.[16] g-C_3N_4 is chemically stable and useful due to its high nitrogen content (60%) and strong covalent bonds between nitrogen and carbon atoms and serves as a potential material for desulfurization[17,18] Many researchers have examined g-C_3N_4's desulfurization of fuel oils.[19–23] Deng and his colleagues recently discovered that (g-C_3N_4) may catalyse oxidative desulfurization.[24] The first part of the investigation showed that (g-C_3N_4)'s low specific surface area and limited active sites hamper its ability to catalyze H_2S to sulfur oxidation. The rational design of unmodified (g-C_3N_4) limits desulfurization processes.[25] Hence, it is important to modify or functionalize carbon or g-C_3N_4 materials with metals, polymers or hetero atoms to enhance their adsorption efficiency. These modifications aid in improving the surface active sites to interact with sulfur compounds through metal–sulfur interaction, inter molecular hydrogen bonding, van der Waals and electrostatic force attraction along with π complexation.[26]

In this regard, positively charged poly(ethyleneimine) [PEI] which contains abundant functional groups (–N, –NH, and NH_2) was used to functionalize the two-dimensional g-C_3N_4 for enhanced adsorptivity. Polyethyleneimine (PEI), a highly branched cationic polymer with primary, secondary, and tertiary amine groups, interacts with g-C_3N_4 owing to its many amino (–NH_2) groups. When PEI is exposed to water in an acidic environment, it is easily protonated thereby acquiring a surface positive charge. PEI is then subsequently utilized to exfoliate bulk g-C_3N_4 to improve its ability to modify the electronic properties of the nanosheets through inter and intra-molecular hydrogen bonding[27] and poly(ethyleneimine)-exfoliated graphitic carbon nitride nanosheets can capture chromium. Kumar and co-workers constructed an environmental covalent organic framework (COF) functionalized with poly(ethyleneimine)[28] for multifunctional applications. PEI as such cannot be used as an adsorbent due to its water soluble nature.[29] PEIs' highly branched reactive amino (–NH_2) group easily crosslinks with epoxide, aldehyde, and hydroxyl groups, forming hydrogels and aerogels.[29] Exfoliating g-C_3N_4 with a bio-degradable polymeric material makes it a non-toxic, bio-compatible and cost-efficient adsorbent material. The incorporation of a biopolymer with reactive functional groups like (–OH, –COOH) such as sodium alginic acid (or sodium alginate SA), fosters an aerogel like texture in the presence of aqueous metal chlorides. SA is useful for hydrogels and aerogel-based adsorbents owing to their crosslinking and ion exchange properties. Sargasso or brown algae produces sodium alginate (SA) consisting of two monomer units, α-L-guluronic acid (G units) and β-D-mannuronic acid (M units), linked by a β-1,4-glycosidic linkage.[30] Physicochemical methods may aid in functionalizing sodium alginate (SA), boosting its adsorption, mechanical strength, and durability. Bahrami *et al.* produced a crosslinked SA/polyacrylamide (PAM) hydrogel that removes methylene blue dye from water and has a satisfactory adsorption capacity.[31] Kurczewska *et al.* created alginate beads with poly-amidoamine-functionalized halloysite nanotubes (Alg/Hal/PAMAM) to adsorb methyl green and sunset yellow colours in water. The Alg/Hal/PAMAM composite may sequentially absorb dyes for removal.[32] Bhattacharyya *et al.* produced an SA/acrylic acid/acrylamide co-polymer to adsorb basic-fuschin and methyl violet dyes in water.[33] Godiya *et al.* reported a sodium alginate-graphitic carbon nitride hydrogel that sequesters methylene blue dye from water, demonstrating excellent adsorption capacity.[34]

Taking into cognizance the above distinct advantages, we propose a straightforward method for self-assembly of poly-(ethyleneimine)-exfoliated graphitic carbon nitride nanosheets (PEI–g-C_3N_4 NSs) impregnated onto calcium alginate beads as a prospective adsorbent for desulfurization. The mesoporous structure offers a high specific surface area of 142 $m^2\ g^{-1}$ and a plethora of functional groups –N, –NH, –NH_2, and –COOH, thereby making it an ideal adsorbent for diesel fuel adsorptive desulfurization. The anchoring of PEI–g-C_3N_4 NSs onto the calcium alginate beads also paves the way for column study in scale-up for real-world application.

2. Material and methods

2.1. Materials

Dibenzothiophene was procured from TCI Chemicals, India, and Melamine, Polyethyleneimine (PEI, M.W., 750 kDa) were obtained from Sigma Aldrich (St Louis, MO, USA). N-hexane and iso-octane (99% pure AR grade) solvents were procured from SRL chemicals, and sodium alginic acid (SA) was procured from Sisco Research Laboratories (SRL) chemicals (from this 5% solution of sodium alginate was made with medium viscosity of 230 mPa s at room temperature). Analytical grade reagents were purchased and used without further purification. Milli-Q water was used for preparing the required solutions.

2.2. Characterization techniques for GPA adsorbent before and after adsorption

To analyse the concentration Dibenzothiophene (model fuel) before and after adsorption using Jasco-V650 UV-Vis spectrometer was used with the path length of 1 cm at wavelength between 200-400 nm. Morphological nature of the gC_3N_4-PEI alginate (GPA) bead composite along with the elemental composition and mapping was characterized using FESEM-EDX from FEI Apreo LoVac scanning electron microscope. SONICS-

Vibra cell (750 W with 40% amplitude) probe sonicator was used to exfoliate gC_3N_4 nanosheets. Crystallinity and X-Ray diffraction pattern of the GPA beads were studied using Rigaku Ultima- IV X-Ray diffractometer with Cu-Kα radiation (1.5405 Å) for a range of 2θ between 5 and 80°. The elemental composition of the adsorbent along with its binding energy variation before and after adsorption of sulfur was characterized by X-ray photoelectron spectroscopy with from Thermo Scientific K-Alpha (Al-Kα monochromator) instrument. The porosity and surface are of the GPA beads before and after adsorption was determined by BET-N_2 isotherm analysis using Microtrac Bel (BEL SORP mini II) BET surface area analyser (GPA beads were degassed at 80 °C for 4 hours; N_2 adsorption). X-ray fluorescence was performed using the PANalytical-Model instrument for qualitative elemental analysis. To confirm the hydrophilic nature of the GPA beads, contact angle instrument from Biolin Scientific-attention theta flex was used. Functional groups of the GPA beads before and after adsorption of sulfur was performed using Attenuated total reflectance (ATR) Alpha II spectrometer, with a room temperature DTGS1 detector. Thermal stability of the gC_3N_4 and GPA beads before and after adsorption was performed using Shimadzu (DTG-60) thermal analyser for a wide range of temperature between 30 and 800 °C. Mechanical properties of the gC_3N_4-PEI alginate composite were inferred using Universal Testing Machine as per ASTM standards from Zwick Roell Z100 with 5 kN load cell at room temperature. The batch adsorption studies, isotherm, kinetics and thermodynamic parameters of the adsorption were performed in Biotecnics Orbital shaker. To measure the sulfur concentration in real diesel using Elementa unicube CHNS analyser. Transmission electron microscopy (TEM; JEM-2100, JEOL, Japan) was used to determine the morphology of the PEI-g-C_3N_4 NSs, calcium alginate beads and also PEI exfoliated g-C_3N_4 NSs@calcium-alginate beads. A 200 kV accelerating voltage was applied to the TEM. The samples of interest were deposited onto TEM grids. The zeta potentials of the adsorbent were measured on a Delsa nano zeta potential analyser (Beckman Coulter Inc., USA). In zeta potential analysis, 658 nm wavelength laser was used 30 mW energy, usually generated by a diode laser.

2.3. Experimental procedure

2.3.1. Synthesis of PEI exfoliated @g-C_3N_4-Nanosheets (PEI-g-C_3N_4 NSs). To prepare a graphitic carbon nitride (g-C_3N_4) 3.0 g of melamine was heated up to 550 °C in a muffle furnace for 5 hours. After cooling down to room temperature, the resultant products were crushed into fine powder. A small portion (1000 mg) of the obtained g-C_3N_4 powder was incubated with HNO_3 (100 mL, 6 M) in a probe ultrasonication process system (UP-100, Chrom Tech Ultrasonic Processor, India) for 6 hours, followed by a purification step by using centrifugation techniques. The exfoliated g-C_3N_4 NSs were then washed several times with Milli-Q water until they reached a neutral pH. The as-made exfoliated g-C_3N_4 NSs were mixed with PEI (50 mg mL^{-1}, 10 mL) in a bath ultrasonicate for 10 hours. The as-formed pale, yellow-colored precipitate was washed several times with Milli-Q water and then dried in an oven at 70 °C.

2.3.2. Synthesis of PEI exfoliated-g-C_3N_4 NSs@calcium-alginate beads. Herein, we used a cross-linking reaction between calcium ions (Ca^{2+}) and sodium alginate (SA) to prepare PEI exfoliated-g-C_3N_4 NSs@calcium alginate beads (Scheme 1). Firstly, 1.0 g of sodium alginate was added to 50 mL of water and then stirred for 4 hours to get a uniform solution. Then, a various amount of PEI exfoliated@g-C_3N_4 NSs was added to the sodium alginic acid (SA) solution under a strong magnetic stir to get a uniform suspension. The mass ratio of PEI exfoliated@g-C_3N_4 NSs and water was 0%, 10%, and 15%, respectively. After that, 3.0 g of calcium chloride ($CaCl_2$) was added to 100 mL of water and then stirred for 24 h to get a uniform solution. Then the PEI exfoliated-g-C_3N_4 NSs@sodium alginate (SA) suspension was dropped into (3.0%, 100 mL) $CaCl_2$ solution by syringe dropper slowly and then waited for 60 mins. Finally, PEI exfoliated@g-C_3N_4 NSs hydrogel alginate beads were formed and then freeze-dried. The as-obtained samples were named to be PEI-g-C_3N_4 NSs@Ca-Alg beads (0%, 5%, and then 10% of Calcium-Alginate beads) (Scheme 1). The average size of the as-formed PEI-g-C_3N_4 NSs@Ca-Alg beads was about 2.5 mm for easier characterizations, the hydrogel microspheres were ground uniformly and then crushed through an 80-mesh sieve. These uniformly obtained alginate beads were characterized and then applied for the adsorptive removal of DBT (sulfur) from model fuel and commercial diesel.

2.3.3. Adsorptive desulfurization procedure. The adsorptive desulfurization of the model fuel (dibenzothiophene in *n*-hexane) was performed conventionally wherein a 50 mL volume of DBT solution (100 mg L^{-1}) was taken in a centrifuge tube, to which 100 mg of unmodified Ca-Alg beads, and PEI–g-C_3N_4-NSs@Ca-Alg beads (adsorbent) were added equilibrated in a vortex shaker at 1300 rpm for 3 h. The initial and final concentration of the DBT was measured using a UV-vis spectrophotometer at λ_{max} 285 nm corresponding to n–π* transitions of the DBT due to the presence of sulfur having two lone pairs of electrons. The decrease in the absorbance at 285 nm confirms the elimination of sulfur in the model fuel, as shown in Fig. S1 (ESI†).

The C_0 and C_e values of DBT in *n*-hexane were quantified by a Jasco V-630 UV-vis spectrometer (JASCO, Japan) at the maximum absorption wavelength of 285 nm for DBT in *n*-hexane.[35] The equilibrium adsorption capacity (q_e) of DBT in *n*-hexane on the adsorbent was calculated from the following mass balance equation:

$$q_e = \frac{(C_0 - C_e)V}{W} \quad (1)$$

where W and V are the weight (g) of the adsorbent and the volume (L) of the contaminated solution, respectively. The removal efficiency (%RE) of the adsorbent for DBT in *n*-hexane was calculated according to the below equation:

$$\%RE = \frac{(C_{initial} - C_e)}{C_{initial}} \times 100 \quad (2)$$

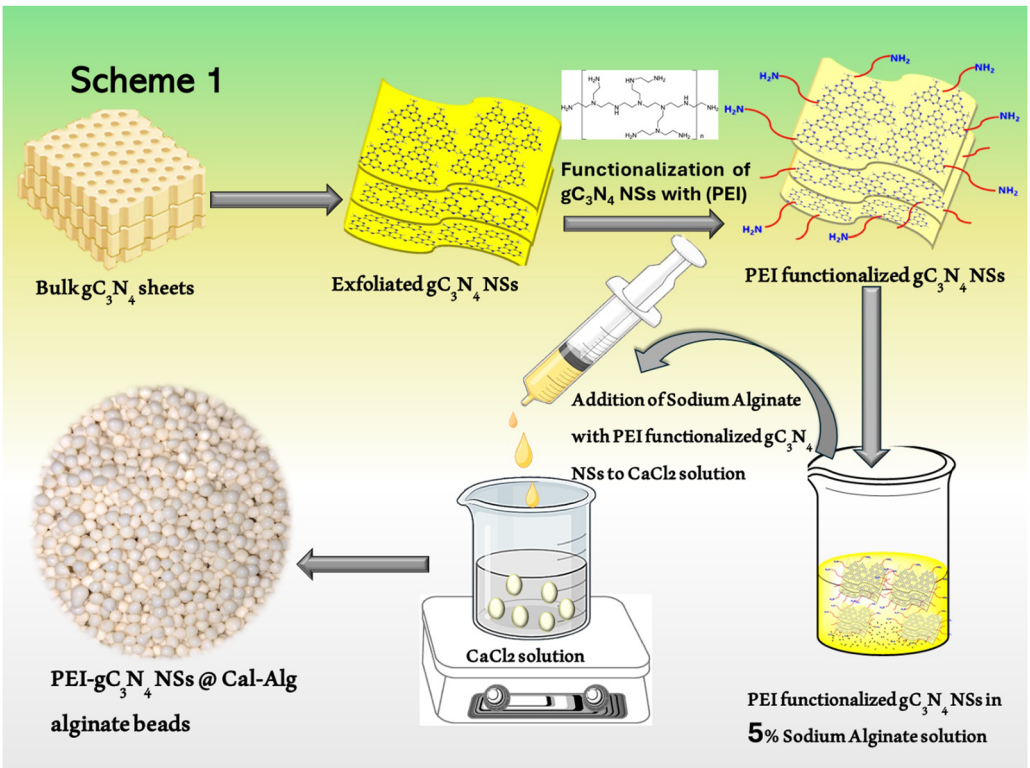

Scheme 1 Schematic representation of the synthesis of PEI-exfoliated g-C_3N_4 nanosheet-based Ca alginate beads.

3. Results and discussion

3.1. Characterizations of adsorbent beads before and after adsorption

The specific surface area and porous nature of the unmodified calcium alginate beads and PEI exfoliated g-C_3N_4 NSs@Cal-alginate bead adsorbent material before and after adsorption of DBT was studied using N_2 adsorption-isotherm studies. The BET curve, as shown in Fig. S2A and C (ESI†), follows a type IV isotherm adhering to the mesoporous nature of the adsorbent. The specific surface area of the as-developed beads was found to be 142.06 $m^2\ g^{-1}$ with a pore volume and diameter of 0.182 $cm^3\ g^{-1}$ and 13.80 nm, respectively. The N_2 uptake of the as-synthesized GPA beads before adsorption of thiophenic compounds was found to be 135 cc g^{-1}, which reduced to 83 cc g^{-1} after the adsorption of the thiophenic compound. The pore volume and the surface area of the beads diminished to 11.08 nm and 35.19 $m^2\ g^{-1}$, respectively (Fig. S2B, D and Table S1, ESI†). Surface area reduction, volume of N_2 uptake in BET studies and the pore diameter of calcium alginate beads after adsorption confirm the adsorbed thiophenic molecules on the surface of the adsorbent material.

The elemental composition and their respective binding energies were determined and analyzed using X-ray photoelectron spectroscopy, as shown in Fig. 1. Fig. 1A demonstrates the presence of C, N, O, Ca, and Cl in PEI-exfoliated g-C_3N_4 NSs, both in their alginate form before and after modification. The survey spectra of the PEI exfoliated g-C_3N_4NSs@Cal–Alg beads were analyzed before and after the adsorption of DBT. The analysis confirmed the existence of aromatic sulphur, as seen in Fig. 1A and B. Fig. 1B illustrates the deconvoluted spectra of S 2p sulfur, with the peaks at 165.6 and 168.4 eV indicating the presence of aromatic sulfur. The N 1s spectra, shown in Fig. 1C, exhibit four clearly identifiable peaks with binding energies of 398.9, 400.2, 401.6, and 406.8 eV. These peaks correspond to the presence of C–N=C, N–(C_3), s(C–NH), and delocalized N^+ groups on the surface of the adsorbent. The binding energy and intensity of C–NH and delocalized N^+ of the PEI exfoliated g-C_3N_4NSs@Cal–Alg beads decreased significantly after sulfur adsorption, indicating electrostatic and hydrogen bonding interactions between these functional groups and DBT molecules.[36] The deconvoluted spectra of C 1s in Fig. 1D exhibit binding energy peaks at 284.9, 285.9, 287.82, and 288.7 eV, which correspond to the presence of C=C, C–O–C/C–OH, C=O, and C–O–NHR bonds in the adsorbent composed of as-developed PEI exfoliated g-C_3N_4 NSs@Cal–Alg beads.[35] Following the adsorption of DBT sulfur compounds, there was a little displacement in the binding energies, resulting in values of 284.5, 285.1, 286.2, and 288.7 eV. The significant reduction in the C=C bond is mostly attributed to the π–π interactions occurring between the layers of PEI–g-C_3N_4 NSs and the aromatic rings of DBT. The spectra of Ca 2p in Fig. 1E exhibit distinct peaks corresponding to the $2p_{1/2}$ and $2p_{3/2}$ energy levels at 351.3 and 348.0 eV, respectively. Following the adsorption of DBT, there was a good shift in these binding energies. The O 1s spectra, shown in Fig. 1F, have clear peaks at 531.6, 538.5, and 533.3 eV, corresponding to O–C/HO–C, C–O–C, and O=C bonds, respectively.[37,38] The interaction of

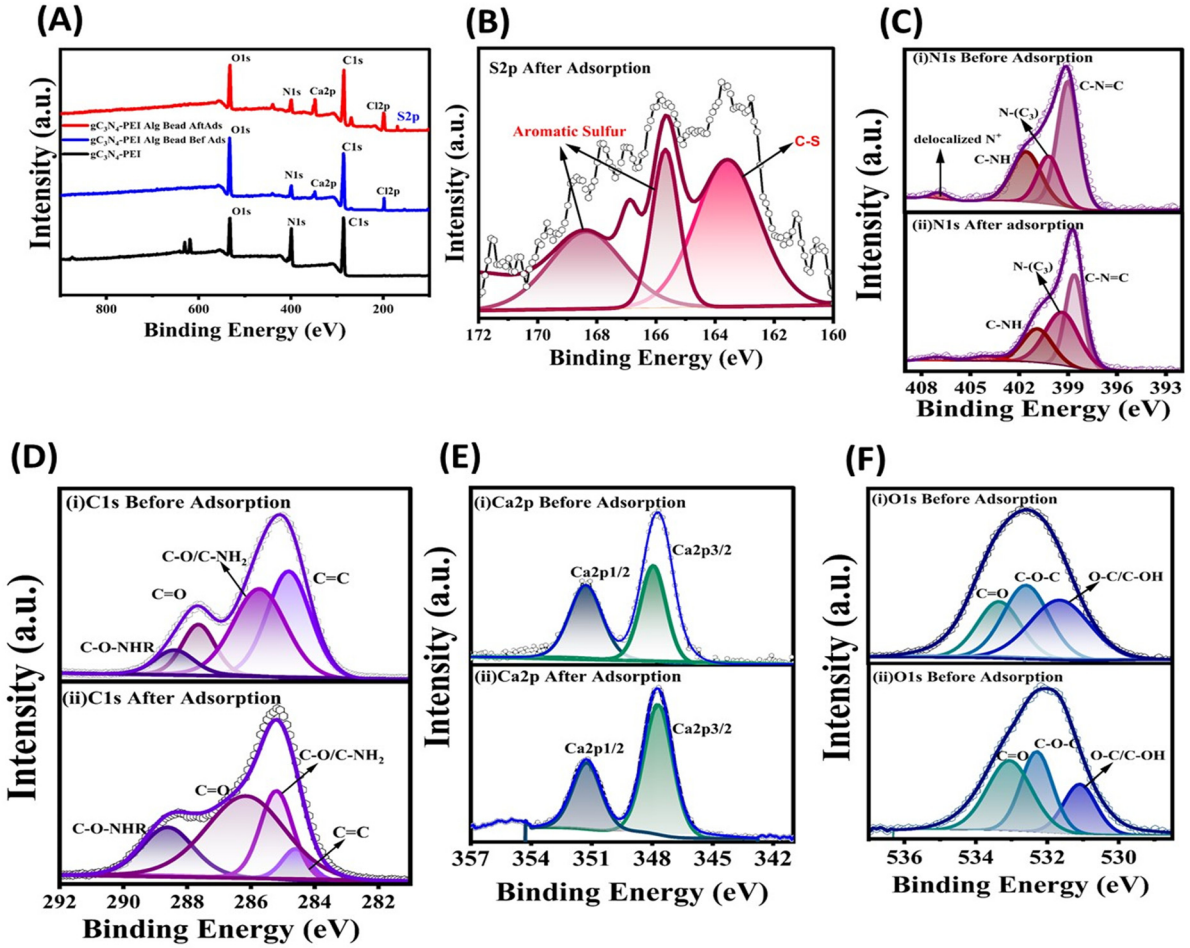

Fig. 1 (A) The total survey spectra of PEI exfoliated g-C_3N_4 NSs, and also PEI exfoliated g-C_3N_4NSs@Cal–Alg beads before and after adsorption of DBT; (B)–(F) high-resolution deconvoluted spectra before and after adsorption of the DBT spectra for sulphur (B), nitrogen (N 1S) (C), carbon spectra C 1S (D), calcium (Ca 2p) spectra (E), and oxygen (O 1S) spectra (F).

oxygen-based functional groups with the electronegative sulfur in the DBT with the GPA beads resulted in a reduction in the binding energy of the O–C bonds to 531.0 eV.

The powder XRD analysis was used to validate the diffraction pattern and graphitic characteristics of the material, as shown in Fig. 2A. The X-ray diffraction (XRD) pattern of melamine and g-C_3N_4 nanosheets (NSs) produced in this study is consistent with the results as previously reported in the literature.[39] The prominent peak seen at an angle of 29.2° corresponds to the crystal plane (002), signifying the high purity of the phase in the g-C_3N_4 NSs. Similarly, the peak at 13.9° corresponds to the (100) plane.[40] The shift in 2θ value was also evident at 27.5° and 12.4° after the functionalization of g-C_3N_4 with PEI. Additionally, the interplanar distance increased marginally from 0.30 nm to 0.32 nm. The perceptible inter-layer expansion in g-C_3N_4 NSs may be attributed to the interaction between the functional groups of PEI and the g-C_3N_4 NSs respectively. The FT-IR spectrum in Fig. 2B was used to ascertain the functional groups and interactions before and after adsorption of DBT (sulfur). The adsorbent exhibited O–H stretching at 3344 cm^{-1}, attributed to the alginate chain bonded with g-C_3N_4 NSs layers by polyethyleneimine. The stretching frequency observed at 1639 cm^{-1} is ascribed to the presence of asymmetric C–O/C=N stretching bands. The stretching frequencies at 1424 and 1098 cm^{-1} correspond to symmetric vibrations of COO stretching and the stretching of the C–O–C group. The band at 690 cm^{-1} implies the C–Cl stretching. The appearance of new bands at 2858 and 874 cm^{-1} upon adsorption may be attributed to the stretching of S–H and S=O groups, indicating the interaction between sulfur and the adsorbent *via* the alginate chain.[41,42] The O–H stretching frequency shifted to 3358 cm^{-1}, and the shift in the C–O/C=N stretching frequencies is attributed to the interaction between the functional groups of the alginate beads and DBT through hydrogen bonding as well as the electronegative sulfur.[43–45] Prior to the adsorption of sulfur, the thermal stability of the adsorbent materials was examined, as seen in Fig. 2D and E. The PEI exfoliated g-C_3N_4 NSs, in their original form, exhibited greater stability when compared to their modified version using alginate beads. The minimal weight loss 100–150 °C corresponds to the water molecules bound to the alginate complex chain followed by a notable weight loss

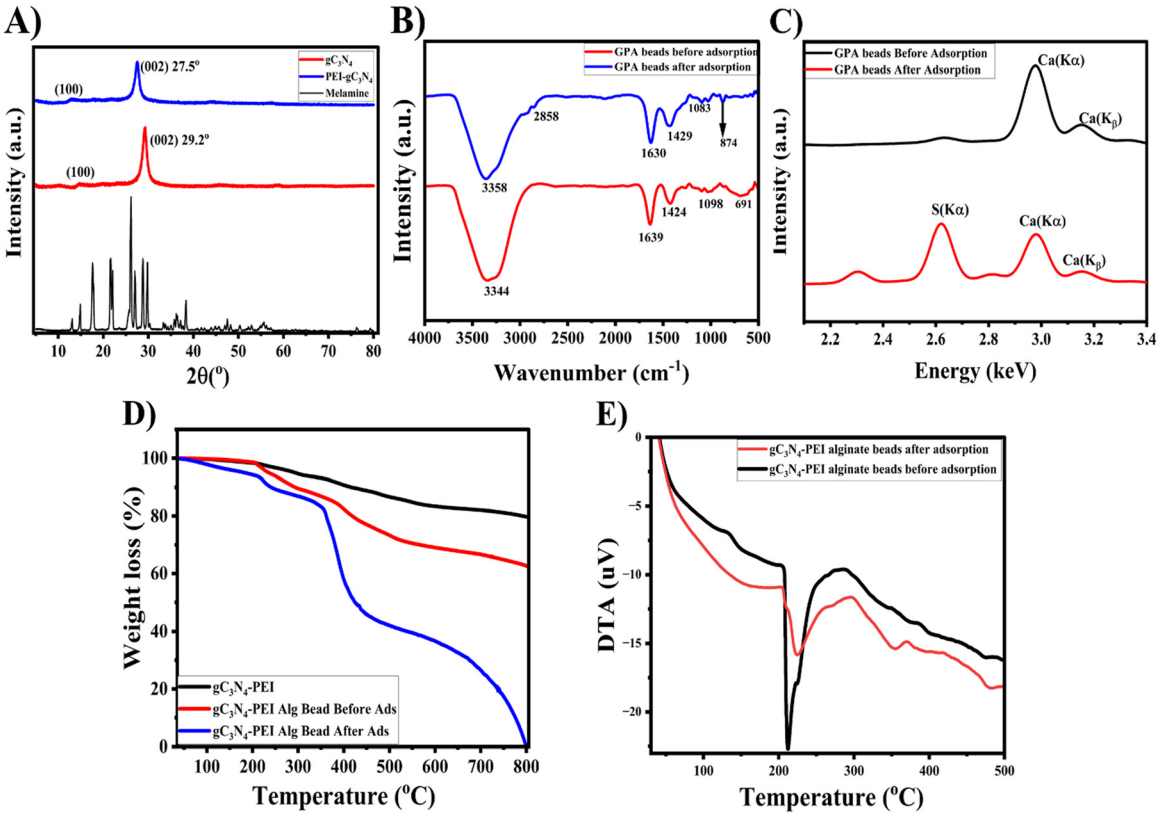

Fig. 2 (A) The powder XRD pattern for melamine (black line), bulk g-C_3N_4 (red line), and PEI exfoliated g-C_3N_4 NSs (dark blue line); (B) the FT-IR spectra for PEI exfoliated g-C_3N_4NSs@Cal–Alg beads (red line) before and after adsorption (dark blue line); (C) X-ray fluorescence (XRF) spectra for PEI exfoliated g-C_3N_4 NSs@Cal–Alg beads (black line) before and after adsorption (red line). (D) The thermogravimetric analysis (TGA) curve for PEI exfoliated g-C_3N_4 NSs (black line), PEI exfoliated g-C_3N_4 NSs@Cal–Alg beads (red line) before and after adsorption (dark blue line); (E) DTA curves for PEI exfoliated g-C_3N_4 NSs@Cal–Alg beads (black line) before and after adsorption (red line).

between 200–250 °C due to the initial degradation of glycosidic linkage in the alginate polymer and corresponds to fragmentation of alginate backbone chain breakage.[46–48] The weight loss % of the GPA beads increased throughout the temperature range of 250–380 °C during the thermal degradation, suggesting the presence of aromatic sulfur compounds on the adsorbent after the removal of sulfur from the model fuel.[49] Quantitative evaluation of elements was conducted using X-ray fluorescence analysis on PEI exfoliated g-C_3N_4 NSs@Cal–Alg beads, both before and after adsorption. The XRF spectrum, shown in Fig. 2C, exhibits a prominent peak at about 3.1 keV, relating to the emissions of Ca (Kα) and Ca (Kβ) both prior to and after adsorption. In addition, a prominent signal at 2.6 keV was seen, indicating the presence of sulfur (S) on the adsorbed surface of the adsorbent (PEI exfoliated g-C_3N_4 NSs@Cal–Alg beads). This confirms that the adsorbent is effective in removing sulfur by adsorptive desulfurization.[50,51]

The as synthesized adsorbent, PEI exfoliated g-C_3N_4NSs (PEI@g-C_3N_4 NSs), unmodified calcium alginate beads (Ca-Alg beads), and calcium alginate beads functionalized with PEI–g-C_3N_4 NSs (Ca-Alg beads@PEI–g-C_3N_4 NSs), were analyzed using transmission electron microscopy (TEM). The TEM images revealed that the PEI–g-C_3N_4 NSs exhibited a small, flat plate-like structure with a smooth surface (Fig. 3A and B). The high-resolution transmission electron microscopy (HR-TEM) image of the PEI–g-C_3N_4 nanosheets (NSs) revealed a distinct and well-defined porosity (Fig. 3C). An analogous feature was detected in structures based on graphitic carbon nitride nanosheets, as reported in previous works.[27] Furthermore, the electron diffraction pattern obtained from the targeted region confirms the crystallinity of the PEI–g-C_3N_4 NSs when observed at a lower magnification (Fig. 3C). In contrast, the calcium alginate beads that were produced had greater elasticity, stretchability, and plasticity, as seen in Fig. 3D. Moreover, this may be attributed to the sodium alginic acid demonstrating increased flexibility. TEM analysis of the PEI–g-C_3N_4 NSs@Ca-Alg beads revealed that they were more flexible, stretchable and mouldable. This is due to their reduced thickness and the structural accumulation resulting from inter and intra-molecular hydrogen bonding. Additionally, the positively charged PEI–g-C_3N_4 NSs interact strongly with the negatively charged alginate at neutral pH. The resulting aggregated product is shown in Fig. 3E and F.

Fig. S3 (ESI†) displays scanning electron microscopy (SEM) images of the individual air-dried and freeze-dried calcium alginate beads (Ca-Alg beads). The air-dried bead had a smooth and plump morphology across its surface, whereas the freeze-dried bead had a granular texture. In addition, the freeze-drying

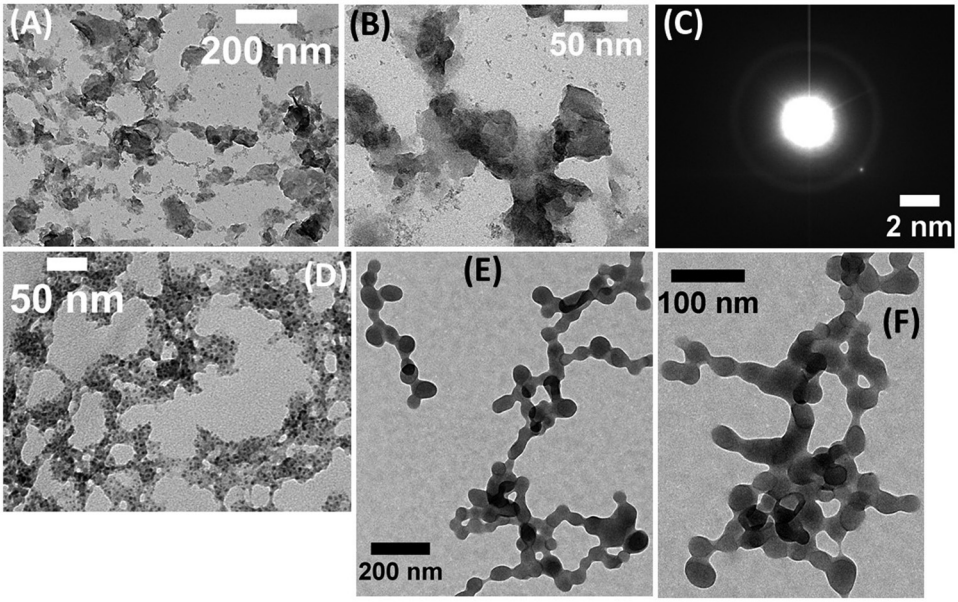

Fig. 3 Transmission electron microscopy (TEM) images of (A) and (B) PEI exfoliated g-C_3N_4 nanosheets (PEI–g-C_3N_4 NSs); (D)–(F) unmodified calcium alginate beads (Ca-Alg beads); (E) and (F) PEI–g-C_3N_4 NSs@Ca-Alg beads; high-resolution transmission electron microscopy (HR-TEM) images of (C) the selected area electron diffraction (SAED) pattern for PEI–g-C_3N_4 NSs.

process caused the moisture to be removed from the beads, resulting in a significant alteration in the surface morphology, which became rough in character. Fig. S3A–C (ESI†) show the FE-SEM images of the air-dried PEI–g-C_3N_4 NSs@Ca-Alg beads after the adsorption of dibenzothiophene (DBT, sulfur). The FE-SEM pictures of the beads following the adsorption of sulfur exhibit no discernible change in the surface morphology, as seen in Fig. S3D–F (ESI†). Fig. S3G (ESI†) EDX analysis and the composition of components confirm the presence of sulfur on the surface of the bead after the adsorption of dibenzothiophene (DBT).

3.1.1. Contact angle measurement. Contact angle measurement was conducted to study whether the material is hydrophilic or hydrophobic. The mean contact angle value of the material $<90^\circ$ refers to a hydrophilic nature and for a value $>90^\circ$ it is said to be hydrophobic.[52,53] For the PEI–g-C_3N_4 NSs@Ca-Alg beads, the contact angle measurement was done using water. The mean contact angle for the PEI–g-C_3N_4 NSs@Ca-Alg beads was found to be 76° as shown in Fig. S4A and B (ESI†). This value affirms the hydrophilic nature of the material.

3.1.2. Mechanical testing. The proposed adsorbent material (PEI–g-C_3N_4 NSs@Ca-Alg beads) for the adsorptive desulfurization is in the form of beads and therefore its mechanical properties such as tensile stress, Young's modulus and compressive stress were studied by mechanical testing using a universal testing machine (UTM). For the tensile stress test, the adsorbent material (5% of PEI, and 15% of PEI) was moulded as a thin film with a dimension of 40 mm in length and 10 mm thickness and performed using ASTM D 3039 standard. This test was done at two different concentrations of polyethyleneimine addition. It was observed that the ultimate tensile strength of the PEI–g-C_3N_4 NSs@Ca-Alg beads with a higher concentration of PEI was found to be 3.5 MPa or 3500 kPa with a Young's modulus of 23.5 MPa (σ/ε). The tensile stress *vs.* strain % curve for the polymer composite material was plotted, as shown in Fig. S4D (ESI†). It was evident from the plot that the stress break was higher for the material with a higher concentration of PEI. This affirms that an increase in the concentration of the PEI improves the ultimate tensile strength and elasticity of the composite material along with the alginate chain. Subsequently, the elongation of the composite material was found to be 280% (calculated from the initial and final length of the sample by utilizing tensile testing). The compression test was conducted with ASTM D695 standard at a speed of 10 mm minute^{-1} with a dimension of 10 mm diameter and 10 mm length. The compressive stress for the as-prepared PEI–g-C_3N_4 NSs@Ca-Alg beads was found to be 0.527 MPa or 527 kPa with a maximum of 80% compressive strain after which the material starts to deform, as shown in Fig. S4C (ESI†). The compressive stress of this proposed PEI–g-C_3N_4 NSs@Ca-Alg bead composite material was found to be comparatively higher than that of earlier reported alginate hydrogel-based materials.

The functional groups and surface charge of the PEI–g-C_3N_4 NSs@Ca-Alg beads were determined by zeta potential analysis. The point of zero charges of Ca-Alg beads@PEI–g-C_3N_4 NSs was determined to be pH_{PZC} = 7.74, and this result signifies that the PEI-modified graphitic carbon nitride can accommodate positive charge with good dispersion of graphitic nanosheets, as indicated in Fig. S4E (ESI†).

3.1.3. Difference in the adsorption efficiency due to the morphological nature of the adsorbents. The PEI–g-C_3N_4 NSs@Ca-Alg beads were dried using two methods: regular

atmospheric air-drying procedures and freeze-drying. Two techniques, air-drying and freeze-drying, were used and evaluated for their effectiveness in adsorptive desulfurization. The experiment included treating 15 mL of a DBT solution with a concentration of 100 mg L^{-1} using 70 mg of adsorbent. The freeze-dried PEI–g-C_3N_4 NSs@Ca-Alg beads showed only 10% DBT adsorption, whereas the air-dried Ca-Alg beads@PEI–g-C_3N_4 NSs exhibited 90% of DBT adsorption and the results are depicted in Fig. S1B and C (ESI†). In addition, the scanning electron microscope (SEM) images of the air-dried and freeze-dried samples were examined, as shown in Fig. S3 (ESI†). It was noted that the surface morphology of the freeze-dried PEI–g-C_3N_4 NSs@Ca-Alg beads seemed to be contracted and rough in texture. Upon closer examination at greater magnification, it was obvious that the surface was smooth, which may explain the lower adsorption of DBT. As a result, the least removal capacity was detected. Consequently, the air-dried PEI–g-C_3N_4 NSs@Ca-Alg beads were then used for conducting the adsorption experiments. The Ca-Alg beads@PEI–g-C_3N_4 NSs, which were air dried, were optimized for the uptake of DBT (100 mg L^{-1}) in *n*-hexane with 40 mL volume and 100 mg adsorbent weight. The results indicated that a maximum removal efficiency of 90% for DBT was attained, as shown in Fig. S1D (ESI†).

3.2. Adsorptive parameters for DBT adsorption

3.2.1. Isotherm studies. To interpret the mechanistic view and the interaction of the adsorbate with the GPA beads, isotherm studies were performed and fitted with different non-linear models. To conduct isotherm investigations, 100 mg amount of PEI–g-C_3N_4 NSs@Ca-Alg beads (as a separate set of experiments) was used. These beads were exposed to varied starting concentrations of DBT ranging from 50–1000 mg L^{-1} in *n*-hexane, which served as the model fuel. The adsorption process was carried out in an orbital shaker at a speed of 120 rpm for a duration of 4 h. The Langmuir isotherm model, which is non-linear, is represented by eqn (3).

$$q_e = q_m K_L \frac{C_e}{1 + K_L C_e} \quad (3)$$

where q_{max} and q_e are the maximum and equilibrium adsorption capacity, K_L is the Langmuir capacity and C_e is the equilibrium concentration reached after the adsorption of DBT in *n*-hexane (model fuel). The model yielded a maximum adsorption capacity of 107.1 mg g^{-1} for PEI exfoliated g-C_3N_4 NSs and 183.03 mg g^{-1} for PEI–g-C_3N_4 NSs@Ca-Alg beads, as shown in Table S2 (ESI†). The R_L value for PEI exfoliated g-C_3N_4 nanosheets as an adsorbent was determined to be 0.16, whereas the R_L value for PEI–g-C_3N_4 nanosheets coated with Ca-Alg beads was discovered to be 0.476. These data confirm the favorable adsorption of DBT in *n*-hexane (a model fuel). The adsorption capacity at equilibrium (q_e) exhibits a significant increase above a concentration of 200 mg L^{-1} (C_e). This suggests that electrostatic attraction and intermolecular hydrogen bonding play a crucial role in the adsorption of DBT molecules. The corresponding data can

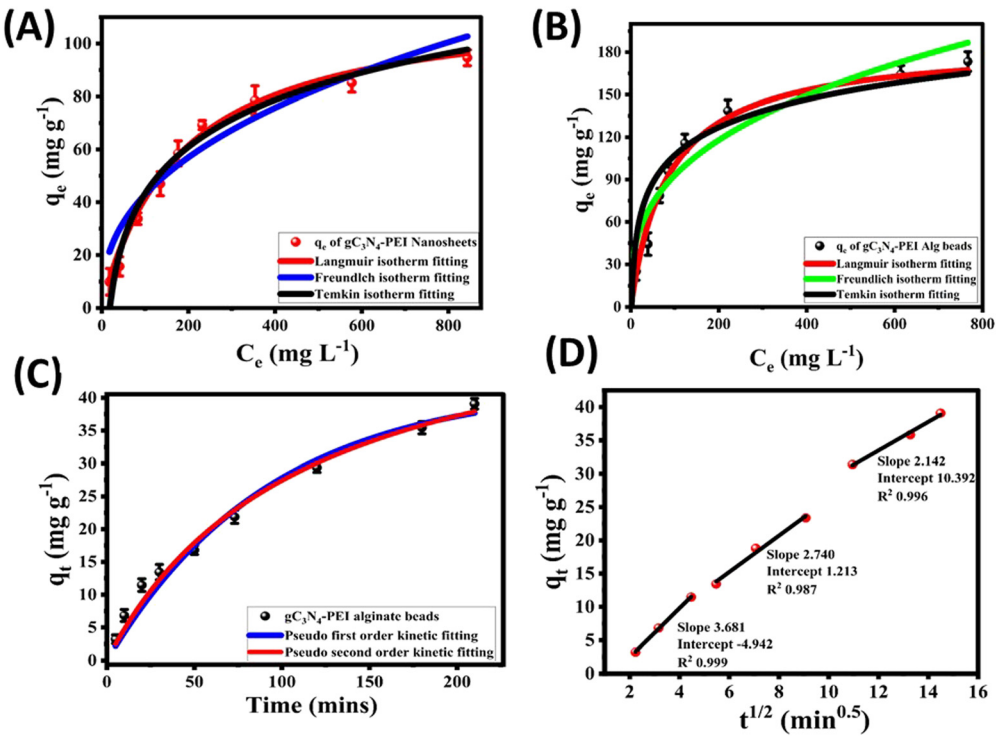

Fig. 4 (A) and (B) Non-linear fitting of the Langmuir (red curve), Freundlich (blue curve) and Temkin isotherms (black curve) for PEI–g-C_3N_4-NSs and calcium alginate beads (Ca-Alg beads) functionalized with PEI–g-C_3N_4 NSs; (C) and (D) calcium alginate beads (Ca-Alg beads) functionalized with PEI–g-C_3N_4 NSs for (C) non-linear pseudo-first-order kinetics and the pseudo-second-order kinetic model for (D) linear plot for intraparticle diffusion.

be seen in Fig. 4A and B. Eqn (4) represents the non-linear Freundlich isotherm model.

$$q_e = K_f C_e^{1/n} \quad (4)$$

where, K_f is the Freundlich constant. The value of n between 1 and 10 implies stronger and more favorable interactions between the adsorbents and DBT molecules. The n value for PEI exfoliated g-C_3N_4 NSs was 1.66, whereas for PEI–g-C_3N_4 NSs@Ca-Alg beads, it was determined to be 1.34. The value of $1/n$, which is closer to 1, shows that the adsorption of DBT molecules by the suggested adsorbent material follows linear adsorption.[54] This suggests that the energies at all adsorption sites are uniform and similar. The corresponding data can be shown in Fig. 4A and B. The Temkin isotherm model is represented by eqn (5),

$$q_e = \frac{RT}{b_{Te}} \ln K_T C_e \quad (5)$$

where K_T is the Temkin isotherm constant in L g^{-1}, R is the gas constant 8.314 J mol^{-1} K^{-1}, b_{Te} is the Temkin constant relating to the heat of adsorption in J mol^{-1}, and T is the absolute temperature in Kelvin. It assumes a uniform distribution of binding energies across the surface of the adsorbent (PEI–g-C_3N_4 NSs@Ca-Alg beads) during the entire adsorption process. This model states that the heat of adsorption decreases as the number of adsorbed DBT molecules on the adsorbent surface increases.

The non-linear isotherm parameters indicated above are shown in Table S2 (ESI†). Comparing the R^2 values of all three isotherm models for both g-C_3N_4-NSs and g-C_3N_4-NSs@Ca-Alg beads, the Langmuir model fits well with the value of 0.98. The adsorption capacity exhibits a significant increase at lower concentrations of DBT due to the abundance of functional groups and adsorption sites. The concentration of the adsorbate DBT molecules intensifies the competition between the adsorbent and the DBT molecules. This competition occurs through the consumption of DBT molecules by the surface functional groups and active sites of the adsorbent.[55] As a result, the adsorption capacity reaches its maximum saturation point at the highest concentration of DBT in n-hexane. The as-prepared adsorbent of PEI–g-C_3N_4NSs@Ca-Alg beads exhibited a greater adsorption capacity.

3.2.2. Kinetics studies on the rate of chemical reactions. The adsorption kinetics were conducted under constant temperature conditions, using an adsorbent dose of 100 mg and a DBT concentration of 100 mg L^{-1} in 50 mL of solution. The experiment was carried out for a duration of 0 to 240 minutes in an orbital shaker operating at 120 rpm. The concentration of the model fuel (DBT in n-hexane) was measured at regular time intervals. The equilibrium concentration (C_e) and adsorption capacity at different time intervals (q_t) were used as experimental data. The non-linear kinetic models, and the resulting plot are given in Fig. 4C. Eqn (6) and (7) represent non-linear pseudo-first order and pseudo-second order kinetic equations.

$$q_e = q_e(1 - e^{k_1 t}) \quad (6)$$

$$q_t = \frac{k_2 q_e^2}{1 + k_2 q_e t} \quad (7)$$

where k_1 and k_2 are the rate constants of first and second-order kinetics. Having a higher adsorption capacity, non-linear models were applied for PEI–g-C_3N_4 NSs@Ca-Alg beads, and it was found that the pseudo-second-order kinetics model fits in terms of their higher regression co-efficient (R^2) which is 0.987 and also the maximum q_e value that is close to the experimentally obtained value is depicted in Fig. 4C, as shown in Table S3 (ESI†). This is in line with the isotherm findings, since the Langmuir isotherm represents physicochemical adsorption and is also applicable to the pseudo-second-order kinetics. Fig. 4D illustrates the Weber–Morris plot of the intra-particle diffusion model, which shows the relationship between q_t and the square root of t. The absorption process consists of three stages. In the first stage, there is diffusion through the boundary layer and the transfer of adsorbate with PEI–g-C_3N_4 NSs@Ca-Alg beads. This is followed by the diffusion of DBT molecules in n-hexane from the boundary layer to the surface of PEI–g-C_3N_4 NSs@Ca-Alg beads, which then enter the bulk phase. During the third stage, the adsorbate molecules interact with the functional groups of PEI–g-C_3N_4 NSs@Ca-Alg beads through electrostatic attraction, hydrogen bonding, and molecular π–π interaction between the g-C_3N_4 NS layers and DBT heterocyclic benzene ring.

3.2.3. Thermodynamics of adsorption. Adsorption is often influenced by temperature and the thermodynamic studies indicate the spontaneity and feasibility of the adsorption system. For thermodynamic study, a 50 mL volume of a solution containing 100 mg L^{-1} of DBT in n-hexane, together with 100 mg of the PEI–g-C_3N_4 NSs@Ca-Alg beads, at various temperatures 298, 308, 318, and 328 K (25 °C, 35 °C, 45 °C, 55 °C) were studied. The mixture was then placed in an orbital shaker, set at a speed of 120 rpm, for a duration of 4 hours. The Van't Hoff plot, which displays the relationship between the natural logarithm of K and the reciprocal of temperature ($1/T$), was generated and is shown in Fig. S4A (ESI†). The intercept and slope of the plot were used to compute the parameters, such as ΔH and ΔS, as shown in Table S4 (ESI†). Eqn (8) represents the van't Hoff linear equation of the plot.

$$\ln K_{eq} = -\frac{\Delta H^o}{R}\left(\frac{1}{T}\right) + \frac{\Delta S^o}{R} \quad (8)$$

The entropy shift (ΔS) was determined to be −0.1364 kJ mol^{-1} K^{-1}, indicating a reduction in spontaneity. The van't Hoff plot has a positive slope, indicating an exothermic adsorption process with a negative change in enthalpy (ΔH). The adsorption efficiency has an inverse relationship with temperature and the change in Gibb's free energy was derived using the equation below for various temperature conditions.

$$\Delta G_r^0 = -RT \ln K_{eq} \quad (9)$$

The obtained ΔG value was −5.168 kJ mol^{-1}, and the negative value of change in Gibb's free energy indicates the spontaneity and feasibility of the reaction.

3.2.4. Adsorbent material regeneration. The desulfurization process of the PEI–g-C_3N_4 NSs@Ca-Alg beads was evaluated by examining their adsorption before and after. Additionally, the regeneration and reusability of the beads were investigated to determine their recycling potential. In order to restore the adsorbent material, the DBT molecules and sulfur compounds that were previously absorbed were removed by desorbing them using a 20 mL solvent of iso-octane. The desorption was examined in the eluent by using a UV-vis spectrophotometer to quantify the concentration of the desorbed DBT (sulfur). In the first cycle, 99% of the sulfur compound DBT was desorbed using PEI–g-C_3N_4 NSs@Ca-Alg beads. The regenerated material was retained for further adsorption cycles, and the procedure was repeated for each subsequent cycle. The PEI–g-C_3N_4 NSs@Ca-Alg beads exhibited excellent reusability, achieving 83% adsorptive desulfurization for up to five cycles, as seen in Fig. S5B (ESI†). However, after five cycles, the adsorption percentage significantly declined. This might be attributed to the unavailability of active sites on the adsorbent for further adsorption investigations.

3.2.5. Fixed bed column adsorption study for adsorptive desulfurization of the model fuel using PEI–g-C_3N_4 NSs@Ca-Alg beads. To assess the efficiency of adsorptive desulfurization, fixed bed column adsorption experiments were performed. To perform this, a column with 30 cm height and 2 cm internal diameter was taken and filled with 4.0 g of adsorbent up to 3 cm bed height. With these column packing parameters, 500 mg L^{-1} of model fuel was passed through the column until the attainment of saturation. Using the experimental data breakthrough curve, the Thomas model and Yoon–Nelson column models were obtained and the respective graphical plots (Fig. 5(A)–(C)).

The linear equation for the Thomas and Yoon–Nelson column model (eqn (10) and (11)) is given as,

$$\ln\left(\frac{C_0}{C_t}-1\right)=\frac{K_{Th}q_o x}{Q}-K_{Th}C_0 t \quad (10)$$

$$\ln\frac{C_t}{C_{0-C_t}}=K_{yn}t-\tau K_{yn} \quad (11)$$

Here, C_0 is the initial concentration, C_t is the concentration of effluent at time 't', K_{Th} is Thomas rate constant, Q is the flow rate, x is the weight of adsorbent beads, K_{yn} is Yoon–Nelson rate constant and τ is the time at which 50% adsorption completed.[56] The theoretically obtained column parameters are given in Table S5 (ESI†). The Thomas model was developed based on the Langmuir isotherm and pseudo-second order kinetics in fixed bed operation.[57,58] The breakthrough curve obtained from experimental data shows that the breakthrough point for adsorptive desulfurization using PEI-g-C_3N_4NSs-Ca alg beads was at 130 min and saturates at 210 min. Fig. 5(B) and (C) show the linear Thomas and Yoon–Nelson model plot from which the maximum adsorption capacity q_o in fixed bed column adsorption was found to be 132.8 mg g^{-1} and the τ (time at which 50% adsorption completed) value was found to be 135 min. The adsorption happens by passing through the boundary layer, followed by mass transfer and diffusion through the pores of the adsorbent. After saturation, the adsorbent was regenerated using toluene–pentane solvent mixture in the ratio 1 : 5, which confirmed the desorption of the sulfur compounds after the fixed bed adsorption. Since the adsorbent material is in the bead form, the column packing and regeneration of the material was not cumbersome and this would find good scale up possibility in industry level application.

3.2.6. Real diesel test to evaluate the effectiveness of adsorptive desulfurization. To evaluate the desulfurization efficiency of PEI–g-C_3N_4NSs@Ca-Alg beads from real commercial diesel, a mixture of 25 mL of commercial diesel and 100 mg of adsorbent was placed in an orbital shaker and agitated at a speed of 120 rpm for a duration of 4 h. The diesel sample was examined for the content of sulfur using a CHNS elemental analyzer, both before and after adsorption. The method was also validated analytically using the calibration obtained with known concentrations of sulfur. Up to 56% of the sulfur present in the actual diesel was successfully eliminated.

3.2.7. Mechanistic view of the adsorptive desulfurization. The as-synthesized PEI–g-C_3N_4 NSs@Ca-Alg beads were used for adsorptive desulfurization of the model fuel and real diesel fuel. The mechanism could be understood through different characterization methods, including HR-TEM, XPS, FT-IR, and powder XRD. Additionally, experimental evidence in the form of isotherm and kinetics data further confirms the effectiveness of this method. The increase in the adsorption efficiency for the

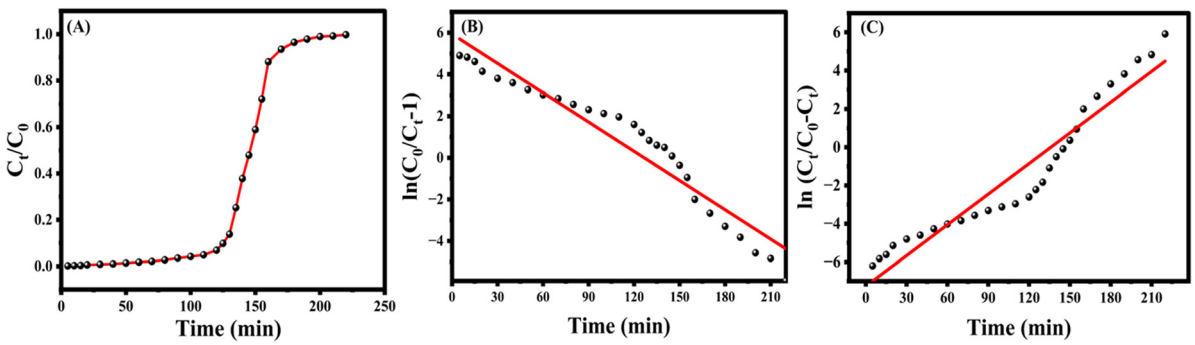

Fig. 5 (A) Thomas model breakthrough curve, (B) linear plot of the Thomas model and (C) linear plot of the Yoon–Nelson model.

alginated form of gC_3N_4–PEI nanosheets could be due to an increase in the functional groups from alginic acid and spacing between the layers of gC_3N_4. The increase in distance between the layers of gC_3N_4 was evident from the XRD pattern (Fig. 2(A)), where there is a decrease in 2θ value which denotes the increase in interplanar distance due to additional functionals on the sides of the g-C_3N_4 layers. The augmentation of the interplanar distance improves the probability of DBT occupancy between layers *via* intercalation processes. Since PEI is a cationic branched polymer, its addition to the g-C_3N_4 sheets also improves the positive charge on the g-C_3N_4 sheets apart from increasing the interplanar distance. This process may also lead to a potential interaction between the g-C_3N_4 layers and DBT rings through π–π complexation. The presence of the C═C sp^2 hybridized bond on the adsorbent surface was clearly shown in the XPS C1s spectra, as depicted in Fig. 1D. Before adsorption, this bond was observed at 284.9 eV, which shifted to 284.5 eV after adsorption of DBT. This change is likely caused by the relatively weak interactions between the lone pair of electrons on the sulfur of the DBT molecule and with the gC_3N_4 layers resulting in a reduction in the binding energy of the C 1s binding energy spectra.[12] In terms of functional groups, the positive amino groups (–N, –NH, $–NH_2$), groups from PEI and –COO groups from the alginate chain efficiently interact with DBT molecules by electrostatic forces and inter molecular hydrogen bonding (Scheme 2). The noteworthy observations were derived from the N 1s and O 1s spectra, as well as the alterations in FT-IR frequencies. The reaction exhibits both Langmuir and Freundlich isotherms, as well as pseudo-second-order kinetics. Additionally, it is characterized as an exothermic process, indicating that it involves physicochemical adsorption. The synergistic impacts of various interaction mechanisms enhance the efficacy of the produced adsorbent (PEI–g-C_3N_4 NSs@Ca-Alg beads) for effectively removing sulfur from both the model fuel and actual diesel fuel.

3.3. Comparison of PEI–g-C_3N_4NSs@Ca-Alg beads with previously reported adsorbent materials for adsorptive desulfurization

The proposed g-C_3N_4NSs@Ca-Alg bead adsorbent material for desulfurization was compared with the previously reported related adsorbent materials with respect to their maximum adsorption capacities, as listed in Table 1. The proposed adsorbent material when compared to the reported g-C_3N_4, alginate bead, porous glass bead and polymer-based materials showed higher adsorption capacity both in batch adsorption and fixed bed adsorption. The synthesis of PEI–g-C_3N_4NSs@Ca-Alg beads was also comparatively economical and eco-friendly. Therefore, the proposed material aids to be an efficient material for adsorptive desulfurization.

4. Conclusion

PEI–g-C_3N_4 NSs@Ca-Alg beads, with functional group abundance, proved to be an effective adsorbent for removing sulfur from model diesel fuel. The adsorbent (PEI–g-C_3N_4 NSs@Ca-Alg beads) exhibited mesoporous characteristics, having a specific

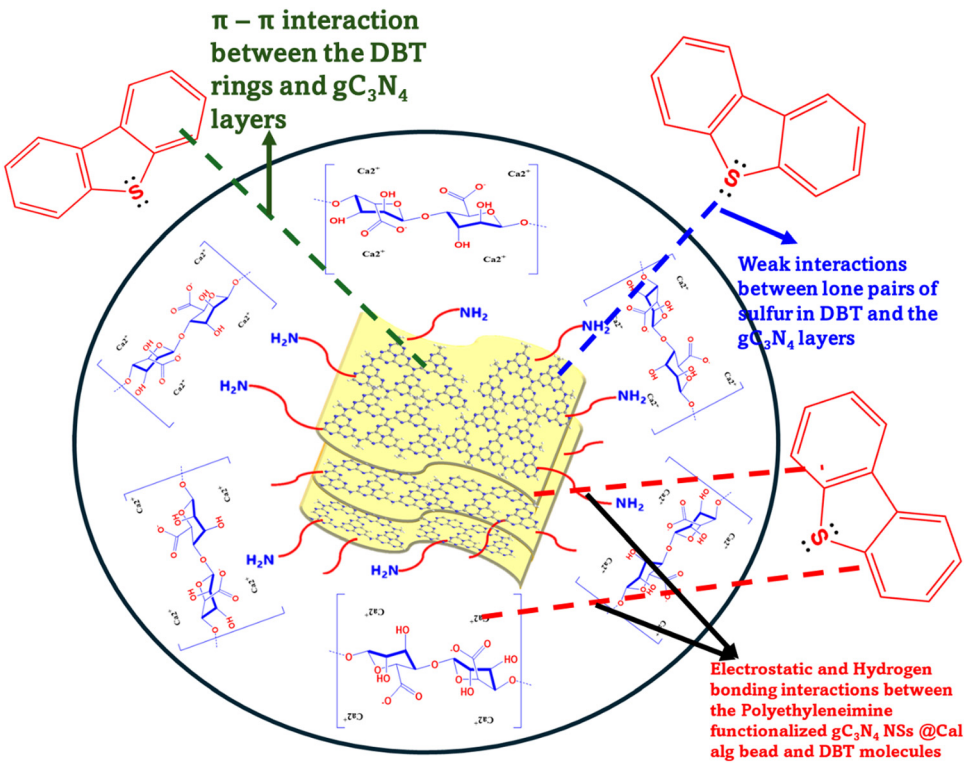

Scheme 2 Schematic representation of the mechanism of adsorptive desulfurization using PEI exfoliated g-C_3N_4 nanosheet based Ca alginate beads.

Table 1 Comparison of PEI–g-C_3N_4NSs@Ca-Alg beads with previously reported adsorbents

Adsorbent materials	Adsorption conditions	q_{max} maximum adsorption capacity (mg g^{-1})	Ref.
Ni-CNF/ACBs	Thiophene (800 mg L^{-1})	88.2	59
PAN-Cu/ABN CNFs	Thiophene (800 mg L^{-1})	74.38	60
Mesoporous g-C_3N_4	Thiophene (400 mg L^{-1})	40.82	61
Ni–WO_3@ g-C_3N_4	DBT (100 mg L^{-1})	48.5	62
N-doped graphene nano adsorbent	DBT (3000 mg L^{-1})	73.4	63
Porous glass beads	DBT (500 mg L^{-1})	10.3	64
N,S doped polybenzoxazine based carbon adsorbent	DBT (500 mg L^{-1})	83.34	65
PET-AC/Cu alginate beads	DBT (500 mg L^{-1})	62.9	66
Cu II-SBA-15 (40)	Thiophene	28.94	67
Co/SBA-15/NH_4F	Benzothiophene	13.55	68
Ordered mesoporous carbon from SBA-16	DBT	29.44	69
PEI–g-C_3N_4 NSs	DBT in *n*-hexane (1000 mg L^{-1})	107.17	Present study
PEI–g-C_3N_4 NSs@Ca-Alg beads	DBT in *n*-hexane (1000 mg L^{-1})	183.03	Present study

surface area of 142 m^2 g^{-1}. The maximum tensile strength and compressive stress of the material indicated the capability to resist 3500 kPa and 527 kPa, respectively, with a strain of 76%. This strain is more than that of the previously reported adsorbent made from alginate-based hydrogel. The batch adsorption process lasted for 240 min, resulting in a 99% removal of sulfur. This reduction brought the sulfur concentration below 10 mg mL^{-1}, in compliance with the standard BS(VI) regulations for sulfur limits. The adsorption capacity of this new adsorbent material was determined to be 183.03 mg g^{-1} following the Langmuir isotherm and pseudo-second-order kinetics. From the thermodynamic variables obtained through the van't Hoff plot, it could be inferred that the adsorption process is exothermic, and spontaneous with a decrease in randomness. The regenerative capability of the adsorbent material was equally good with a removal efficiency of 80% for up to five cycles. The PEI–g-C_3N_4 NSs@Ca-Alg bead adsorbent demonstrated the capability to progressively eliminate 56% of sulfur from the commercial diesel. In summary, the PEI–g-C_3N_4 NSs@Ca-Alg beads find valuable application towards the desulfurization of fuel.

Author contributions

N. Rajesh and Himanshu Aggarwal were involved in conceptualization of the work and M. Christina Nilavu performed all the experiments related to adsorption. Christina Nilavu was also involved in acquiring data for all analytical characterizations. A. Santhana Krishnakumar was involved in studies and interpretations pertaining to analytical characterizations and manuscript writing.

Data availability

The datasets generated during and/or analysed during the current study are not publicly available due to confidentiality of the results, but are available from the authors on reasonable request.

Conflicts of interest

The authors declare that they have no known competing financial interests or personal relationships that could have appeared to influence the work reported in this paper.

Acknowledgements

The authors acknowledge the Central Analytical Laboratory, BITS Pilani, Hyderabad Campus, India for their support in the analytical characterization techniques. Himanshu Aggarwal thanks DST-SERB for funding (grant sanction order number CRG/2022/004414).

References

1 S. Xun, R. Le, C. Hu, D. Liu, S. Wang, M. He, W. Zhu and H. Li, *Energy Fuels*, 2023, **37**, 6276–6280.
2 S. S. Shah, I. Ahmad, W. Ahmad, M. Ishaq and H. Khan, *Energy Fuels*, 2017, **31**, 7867–7873.
3 E. Svinterikos, I. Zuburtikudis and M. Al-Marzouqi, *J. Nanotechnol.*, 2019, **2019**, 2809867.
4 A. Tanimu, G. Tanimu, S. A. Ganiyu, Y. Gambo, H. Alasiri and K. Alhooshani, *Energy Fuels*, 2022, **36**, 3394–3419.
5 A. Yaghoot-Nezhad, M. Moradi, M. Rostami, I. Danaee and M. R. Khosravi-Nikou, *Energy Fuels*, 2020, **34**, 13588–13605.
6 S. Xia, L. Zhang, A. Davletshin, Z. Li, J. You and S. Tan, *Polymers*, 2020, **12**, 1–36.
7 L. Motlagh, S. Shabani and S. Ghaderzadeh, *Adsorption*, 2024, **30**, 1153–1160.
8 M. Christina Nilavu, B. Arunraj, H. Aggarwal and N. Rajesh, *Fuel*, 2022, **324**, 124472.
9 M. Christina Nilavu, B. Arunraj, H. Aggarwal and N. Rajesh, *Fuel*, 2023, **345**, 128172.
10 S. Sonal, P. Prakash, B. K. Mishra and G. C. Nayak, *RSC Adv.*, 2020, **10**, 13783–13798.
11 L. Ullah, G. Zhao, N. Hedin, X. Ding, S. Zhang, X. Yao, Y. Nie and Y. Zhang, *Chem. Eng. J.*, 2019, **362**, 30–40.
12 M. C. Nilavu, T. Leelasree, H. Aggarwal and N. Rajesh, *Sustainable Energy Fuels*, 2024, **8**, 1679–1690.

13 F. F. Roman, J. L. Díaz De Tuesta, A. M. T. Silva, J. L. Faria and H. T. Gomes, *Catalysts*, 2021, **11**, 1–41.
14 N. Zhou, X. Huang, Y. Zhang, J. He and X. Zhang, *Appl. Surf. Sci.*, 2018, **448**, 636–641.
15 G. Lei, Y. Cao, W. Zhao, Z. Dai, L. Shen, Y. Xiao and L. Jiang, *ACS Sustainable Chem. Eng.*, 2019, **7**, 4941–4950.
16 M. He, W. Zhu, S. Xun, Q. Ti, Z. Jiao, L. Wu, L. Chen, L. Zhu and H. Li, *Ind. Eng. Chem. Res.*, 2020, **59**, 18471–18479.
17 M. Saeed, M. Munir, A. Intisar and A. Waseem, *ACS Omega*, 2022, **7**, 15809–15820.
18 L. Shen, G. Lei, Y. Fang, Y. Cao, X. Wang and L. Jiang, *Chem. Commun.*, 2018, **54**, 2475–2478.
19 X. Li, X. Yang, F. Zhou, J. Zhang, H. Yang, Y. Wang, Y. Zhao, X. Yuan, J. Ju and S. Hu, *J. Taiwan Inst. Chem. Eng.*, 2019, **100**, 210–219.
20 M. Yuan, H. Yuan, S. Xun, R. Le, Y. Huang, M. He, L. Zhu, W. Zhu and H. Li, *Fuel*, 2022, **319**, 123792.
21 J. Yang, W. Ma, M. Li, F. He, H. Zhang and H. Zhang, *Inorg. Chem. Commun.*, 2022, **138**, 109268.
22 Z. Yu, X. Huang, S. Xun, M. He, L. Zhu, L. Wu, M. Yuan, W. Zhu and H. Li, *J. Mol. Liq.*, 2020, **308**, 113059.
23 X. Liu, J. Li, Y. Guo, J. Wu and B. Hu, *React. Chem. Eng.*, 2022, **7**, 1380–1390.
24 C. Deng, Y. Lv, M. Sun, M. Yaseen, S. Li and L. Wang, *J. Environ. Chem. Eng.*, 2024, **12**, 111707.
25 S. Xun, Q. Ti, L. Wu, M. He, C. Wang, L. Chen, W. Yang, L. Zhu, W. Zhu and H. Li, *Energy Fuels*, 2020, **34**, 12379–12387.
26 C. Sun, F. Pan and H. Bin, *et al.*, *Nat. Commun.*, 2018, **9**, 743.
27 E. Arputharaj, A. S. Krishna Kumar, W. L. Tseng, S. J. Jiang, Y. L. Huang and H. U. Dahms, *Langmuir*, 2021, **37**, 7147–7155.
28 A. S. Krishna Kumar, W. Bin Tseng, E. Arputharaj, P. J. Huang, W. L. Tseng and T. Bajda, *ACS Sustainable Chem. Eng.*, 2023, **11**, 6956–6969.
29 A. S. Krishna Kumar, J. Warchol, J. Matusik, W. L. Tseng, N. Rajesh and T. Bajda, *npj Clean Water*, 2022, **5**, 1–12.
30 L. Fan, Y. Lu, L. Y. Yang, F. Huang and X. Kun Ouyang, *J. Colloid Interface Sci.*, 2019, **554**, 48–58.
31 Z. Bahrami, A. Akbari and B. Eftekhari-Sis, *Int. J. Biol. Macromol.*, 2019, **129**, 187–197.
32 J. Kurczewska, M. Cegłowski and G. Schroeder, *Int. J. Biol. Macromol.*, 2019, **123**, 398–408.
33 R. Bhattacharyya and S. K. Ray, *J. Ind. Eng. Chem.*, 2015, **22**, 92–102.
34 C. B. Godiya, Y. Xiao and X. Lu, *Int. J. Biol. Macromol.*, 2020, **144**, 671–681.
35 U. Arellano, J. A. Wang, M. T. Timko, L. F. Chen, S. P. Paredes Carrera, M. Asomoza, O. A. González Vargas and M. E. Llanos, *Fuel*, 2014, **126**, 16–25.
36 T. Wang, L. X. Wang, D. L. Wu, W. Xia and D. Z. Jia, *Sci. Rep.*, 2015, **5**, 1–9.
37 L. Tan, J. Xu, X. Zhang, Z. Hang, Y. Jia and S. Wang, *Appl. Surf. Sci.*, 2015, **356**, 447–453.
38 G. Raptopoulos, M. Papastergiou, D. Chriti, E. Effraimopoulou, T. Čendak, N. Samartzis, G. Mali, T. Ioannides, P. Gurikov, I. Smirnova and P. Paraskevopoulou, *Mater. Adv.*, 2021, **2**, 2684–2699.
39 M. R. Islam, A. K. Chakraborty, M. A. Gafur, M. A. Rahman and M. H. Rahman, *Res. Chem. Intermed.*, 2019, **45**, 1753–1773.
40 Y. Zhang, Q. Pan, G. Chai, M. Liang, G. Dong, Q. Zhang and J. Qiu, *Sci. Rep.*, 2013, **3**, 1–8.
41 W. R. Feairheller and J. E. Katon, *Spectrochim. Acta*, 1964, **20**, 1099–1108.
42 X. Zhu, M. Su, S. Tang, L. Wang, X. Liang, F. Meng and Y. Hong, *Mol. Vis.*, 2012, 1973–1982.
43 N. Yang, R. Wang, P. Rao, L. Yan, W. Zhang, J. Wang and F. Chai, *Crystals*, 2019, **9**, 255.
44 G. Balkız, E. Pingo, N. Kahya, H. Kaygusuz and F. Bedia Erim, *Water, Air, Soil Pollut.*, 2018, **229**, 131.
45 A. Li, Y. Qiao, X. Jiang, M. Zhao and L. Zhao, *Dalton Trans.*, 2022, **51**, 15842–15853.
46 Y. Liu, Y. Li, L. Yang, Y. Liu and L. Bai, *Iran. Polym. J.*, 2005, **14**, 457–463.
47 C. G. Flores-Hernández, M. de los A. Cornejo-Villegas, A. Moreno-Martell and A. Del Real, *Polymers*, 2021, **13**, 1–12.
48 J. P. Soares, J. E. Santos, G. O. Chierice and E. T. G. Cavalheiro, *Ecletica Quim.*, 2004, **29**, 57–63.
49 S. M. Elbayomi, H. Wang, T. M. Tamer and Y. You, *Polymers*, 2021, **13**, 2575.
50 S. O. Dima, D. M. Panaitescu, C. Orban, M. Ghiurea, S. M. Doncea, R. C. Fierascu, C. L. Nistor, E. Alexandrescu, C. A. Nicolae, B. Trica, A. Moraru and F. Oancea, *Polymers*, 2017, **9**, 374.
51 S. A. M. Hesp and H. F. Shurvell, *Int. J. Pavement Eng.*, 2010, **11**, 541–553.
52 S. Rasouli, N. Rezaei, H. Hamedi, S. Zendehboudi and X. Duan, *Mater. Design*, 2021, **204**, 109599.
53 R. Anand Omar, B. Bhaduri and N. Verma, *Mater. Lett.*, 2024, **361**, 136117.
54 J. Febrianto, A. N. Kosasih, J. Sunarso, Y. H. Ju, N. Indraswati and S. Ismadji, *J. Hazard. Mater.*, 2009, **162**, 616–645.
55 A. Li, H. Deng, C. Ye and Y. Jiang, *ACS Omega*, 2020, **5**, 15152–15161.
56 S. Koppula, P. Jagasia, M. K. Panchangam and S. B. Manabolu Surya, *J. Solid State Chem.*, 2022, **312**, 123168.
57 C. G. Lee, J. H. Kim, J. K. Kang, S. B. Kim, S. J. Park, S. H. Lee and J. W. Choi, *Desalin. Water Treat.*, 2015, **55**, 1795–1805.
58 O. B. Omitola, M. N. Abonyi, K. G. Akpomie and F. A. Dawodu, *Appl. Water Sci.*, 2022, **12**, 1–9.
59 Y. N. Prajapati and N. Verma, *Fuel*, 2017, **189**, 186–194.
60 X. L. Sun, Z. Liu and Z. L. Cheng, *J. Alloys Compd.*, 2021, **885**, 160976.
61 X. Huang, Y. Zhang, Y. Lai and Y. Li, *J. Sulfur Chem.*, 2021, **43**, 156–168.
62 M. Saeed, M. Munir, A. Intisar and A. Waseem, *ACS Omega*, 2022, **7**, 15809–15820.
63 S. S. Meshkat, A. Rashidi, Z. H. Dastgerdi and M. D. Esrafili, *Ecotoxicol. Environ. Saf.*, 2019, **172**, 89–96.
64 C. Shen, Y. J. Wang, J. H. Xu, Y. C. Lu and G. S. Luo, *Green Chem.*, 2012, **14**, 1009–1015.
65 R. Zhao, Z. Jin, J. Wang, G. Zhang, D. Zhang, Y. Sun, T. Guan, J. Zhao and K. Li, *Fuel*, 2018, **218**, 258–265.

66 M. Fayazi and M. Ghanei-Motlagh, *J. Colloid Interface Sci.*, 2021, **604**, 517–525.
67 L. Kong, T. Zhang, R. Yao, Y. Zeng and L. Zhang, *Microporous Mesoporous Mater.*, 2017, **251**, 69–76.
68 L. M. Correia, J. A. Cecilia, F. Murilo, T. De Luna and E. Vilarrasa-garc, *Can. J. Chem. Eng.*, 2017, **95**, 2315–2323.
69 M. Anbia and S. Karami, *J. Nanostruct. Chem.*, 2015, **5**, 131–137.